

Directional Growth of Human Neuronal Axons in a Microfluidic Device with Nanotopography on Azobenzene-Based Material

Mervi Ristola, Chiara Fedele, Sanna Hagman, Lassi Sukki, Fikret Emre Kapucu, Ropafadzo Mzezewa, Tanja Hyvärinen, Pasi Kallio, Arri Priimagi, and Susanna Narkilahti*

Axonal dysfunction and degeneration are important pathological features of central nervous system (CNS) diseases and traumas, such as Alzheimer's disease, traumatic brain injury, ischemic stroke and spinal cord injury. Engineered microfluidic chips combined with human pluripotent stem cell (hPSC)-derived neurons provide valuable tools for targeted *in vitro* research on axons to improve understanding of disease mechanisms and enhance drug development. Here, a polydimethylsiloxane (PDMS) microfluidic chip integrated with a light patterned substrate is utilized to achieve both isolated and unidirectional axonal growth of hPSC-derived neurons. The isolation of axons from somas and dendrites and robust axonal outgrowth to adjacent, axonal compartment, is achieved by optimized cross-sectional area and length of PDMS microtunnels in the microfluidic device. In the axonal compartment, the photoinscribed nanotopography on a thin film of azobenzene-containing molecular glass efficiently guides the growth of axons. Integration of nanotopographic patterns with a compartmentalized microfluidic chip creates a human neuron-based model that supports superior axonal alignment in an isolated microenvironment. The practical utility of the chip by studying oxygen-glucose deprivation-induced damage for the isolated and aligned axons is demonstrated here. The created chip model represents a sophisticated platform and a novel tool for enhanced and long-term axon-targeted *in vitro* studies.

1. Introduction

The polarized morphology of neurons allows the transmission of neuronal signals along long, slender axons over extended distances. The dysfunction and degeneration of axons are important hallmarks of many neurological disorders and traumas ranging from spinal cord injury to neurodegenerative diseases such as Alzheimer's disease. Thus, targeted research on axons is of great importance for improving the understanding of central nervous system (CNS) diseases and developing treatments for these devastating conditions, many of which lack disease-alleviating or disease-preventing therapies.^[1,2] Human pluripotent stem cell (hPSC)-derived neural cells hold great promise for *in vitro* disease modeling and drug discovery for CNS diseases.^[3,4] hPSCs provide an unlimited cell source for producing several types of neurons, and induced pluripotent stem cell (iPSC) technology enables the generation of patient-derived neurons that can recapitulate disease characteristics *in vitro*.^[5,6] hPSC-based models have been used to study CNS diseases associated with axonal dysfunction and degeneration.^[7–9] However, the full potential of *in vitro* modeling requires combining hPSC biology with state-of-the-art engineering technologies.


Axonal research has been remarkably accelerated by the development of engineered *in vitro* devices that guide the organization of neurons, allowing the isolation of the axonal microenvironment. These compartmentalized devices enable precise spatial control, for example, targeted monitoring, measurement, and manipulation of axons, which are unfeasible or difficult to perform with conventional *in vitro* culture systems or *in vivo*.^[10–12] The first devices used for neuron compartmentalization were Campenot chambers, which use a Teflon ring for the separation of neuronal somas and axons.^[13–15] These were followed by microfluidic polydimethylsiloxane (PDMS)-based devices, which currently represent the most common device type owing to their ease of fabrication and possibility of producing complex and highly controllable devices.^[10,11,16–19] Axonal isolation in PDMS microfluidic devices is based on microtunnels whose dimensions allow the passage of axons

in vitro.^[5,6] hPSC-based models have been used to study CNS diseases associated with axonal dysfunction and degeneration.^[7–9] However, the full potential of *in vitro* modeling requires combining hPSC biology with state-of-the-art engineering technologies.

Axonal research has been remarkably accelerated by the development of engineered *in vitro* devices that guide the organization of neurons, allowing the isolation of the axonal microenvironment. These compartmentalized devices enable precise spatial control, for example, targeted monitoring, measurement, and manipulation of axons, which are unfeasible or difficult to perform with conventional *in vitro* culture systems or *in vivo*.^[10–12] The first devices used for neuron compartmentalization were Campenot chambers, which use a Teflon ring for the separation of neuronal somas and axons.^[13–15] These were followed by microfluidic polydimethylsiloxane (PDMS)-based devices, which currently represent the most common device type owing to their ease of fabrication and possibility of producing complex and highly controllable devices.^[10,11,16–19] Axonal isolation in PDMS microfluidic devices is based on microtunnels whose dimensions allow the passage of axons

Dr. M. Ristola, Dr. S. Hagman, Dr. F. E. Kapucu, R. Mzezewa, Dr. T. Hyvärinen, Dr. S. Narkilahti
Neuro Group
Faculty of Medicine and Health Technology
Tampere University
Arvo Ylpön katu 34, Tampere 33520, Finland
E-mail: susanna.narkilahti@tuni.fi

Dr. C. Fedele, Prof. A. Priimagi
Smart Photonic Materials Group
Faculty of Engineering and Natural Sciences
Tampere University
Korkeakoulunkatu 10, Tampere 33720, Finland
L. Sukki, Prof. P. Kallio
Micro- and Nanosystems Research Group
Faculty of Medicine and Health Technology
Tampere University
Korkeakoulunkatu 10, Tampere 33720, Finland

 The ORCID identification number(s) for the author(s) of this article can be found under <https://doi.org/10.1002/admi.202100048>.

© 2021 The Authors. Advanced Materials Interfaces published by Wiley-VCH GmbH. This is an open access article under the terms of the Creative Commons Attribution License, which permits use, distribution and reproduction in any medium, provided the original work is properly cited.

DOI: 10.1002/admi.202100048

from the initial cell compartment to the adjacent compartment while restricting the migration of the somas, hence keeping them in the initial cell compartment.^[12,20,21] Rodent neurons have been extensively used in these devices, and past studies have increased our knowledge about axon biology and pathology related to, for example, axonal behavior, guidance and transport, and synapse formation.^[10,20,22–27] Much less data is available for hPSC-derived neurons,^[28–31] and it is well known that species-dependent differences prevent the generalization of the results obtained with rodent cells. Thus, there is an acknowledged need to create human neuron-based compartmentalized devices to better model human neurological diseases associated with axonal injury in vitro.

Microtunnels are micron-scale structures that promote aligned axonal growth inside tunnels. However, the compartments connected to microtunnels comprise much larger areas whose edge lengths are usually at the millimeter scale. Thus, as axons enter the compartment designed for axonal isolation, they tend to lose their aligned orientation and grow in random directions.^[20,21,24,29,32] For targeted research on axons, a compartment containing well-defined, aligned axons in the absence of somas is important because this enhances monitoring of axon-specific cellular and subcellular events and facilitates the experimental analysis. In one study conducted with rodent neurons, partially sealed microgrooves patterned on a PDMS substrate were used to generate isolated axons simultaneously with their guided growth in straight lines.^[33] Topographical patterns on PDMS and Nafion substrates also guide the aligned growth of axons of hPSC-derived neurons. Such results, however, have been reported only in non-compartmentalized culture systems,^[34–37] which lack the advantages of compartmentalized devices with isolated axonal microenvironments. Furthermore, all the reported studies have had a follow-up time shorter than three weeks, which may be a limiting factor when modeling relatively slowly progressive CNS diseases in vitro.

In this study, we demonstrate the robust isolation of axons of hPSC-derived and primary rat neurons in a microfluidic device through extensive screening of optimal PDMS microtunnel dimensions. As a new approach for axonal guidance of hPSC-derived neurons, we integrate a light-responsive azobenzene-containing material (referred to as DR1-glass hereafter) into the microfluidic device. In response to structured light irradiation, this material can reversibly change its surface topography due to azobenzene photoisomerization.^[38] This allowed us to create a novel axonal model consisting of a compartmentalized microfluidic chip with microtunnels coupled with a topographically patterned nanostructured surface for modulating axonal growth within their own microenvironment. We verified that this engineered model for hPSC-derived neurons resulted in superior axonal isolation and alignment in the desired direction, which was maintained for at least six weeks. The aligned axons showed quantifiable degeneration when oxygen-glucose deprivation (OGD) was introduced to the cells cultured in the chip. This is a relevant in vitro model for axon-targeted research that combines both *axonal isolation* from somas using a microtunnel technique and *axonal alignment* using an interference lithography technique for patterned DR1-glass resulting in the compartmentalized aligned axons, an outcome that could not

be achieved with using just one of the techniques. The model may have high significance for both studying the mechanisms of axon biology in health and disease and for drug screening and development for CNS diseases, while the light responsiveness of the DR1-glass allows the study of axonal growth and development in dynamic conditions.

2. Results

2.1. Axon Extension and Compartmentalization by Using PDMS Microtunnels

First, we investigated axon extension and compartmentalization in a microtunnel testing device we developed that comprised a neuron compartment and axon chambers separated by microtunnels (Figure 1a–c). Two microtunnel heights and three microtunnel lengths were tested in six different combinations (height/length in μm —1/100, 1/250, 1/500, 3.5/100, 3.5/250, and 3.5/500) to optimize the microtunnel size for hPSC-derived cortical neurons. After seeding, hPSC-derived neurons (human embryonic stem cell (hESC) line Regea 08/017) started to migrate from the cell seeding area (Figure 1a), and the neuronal processes reached the entry of the microtunnels (shown with an arrow) within a few days in all devices (Figure 2a). All the microtunnel dimensions allowed the

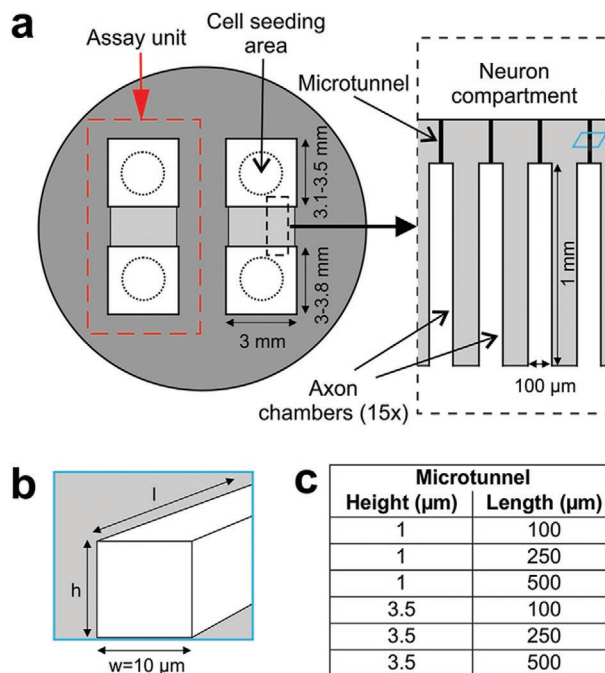


Figure 1. Schematic illustration of the microfluidic microtunnel testing device used to study axonal isolation and extension. a) The device contains two identical assay units; one is highlighted with a red dashed box. One assay unit consists of the neuron compartment and 15 axon chambers, each of which is interconnected with the neuron compartment by a single microtunnel. The outer diameter of the device is 15 mm, and the height is 3 mm. b) A cross-section of the microtunnel (shown in the blue box in Figure 1a). c) Tested microtunnel dimensions with a constant tunnel width of 10 μm . w = width, h = height, l = length.

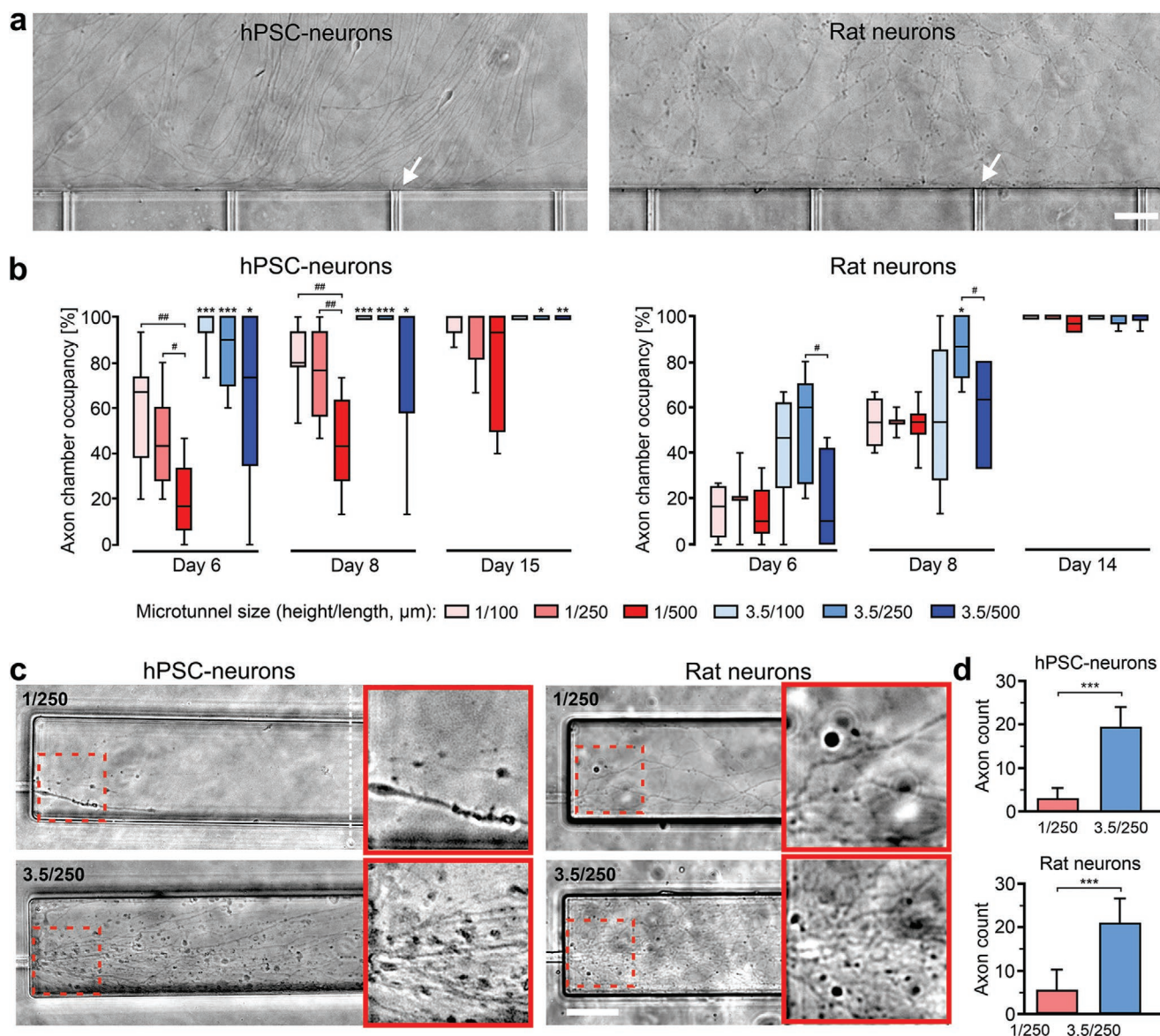


Figure 2. Axon extension and compartmentalization via microtunnels in the microtunnel testing device. a) Representative phase-contrast images of human PSC-derived (hESC line Regea 08/017) and primary rat cortical neurons extending their processes towards the entry of microtunnels (arrows) in the device with 3.5/250 microtunnels. b) Axon chamber occupancy (%) indicating the number of axon chambers containing axons in one assay unit of the microtunnel testing device for human and rat neurons. All analyzed time points are shown in Figure S1, Supporting Information. The data are shown as box plots with min-max whiskers. For human neurons, 8–12 assay units are analyzed from two independent experiments. For rat neurons, a representative experiment with 2–6 assay units is shown and the experiment is performed twice, which showed a similar trend in the results. Statistical analyses are calculated using the Mann-Whitney U-test; * symbols indicate significant differences compared to the 1 μm high microtunnel of the same length and # symbols indicate comparisons between different tunnel lengths with the same height; * $p < 0.05$, ** $p < 0.01$, *** $p < 0.001$, # $p < 0.05$, and ## $p < 0.01$. c) Representative phase-contrast images showing axons of human (day 16) and rat (day 14) neurons extending into the axon chambers with 1/250 and 3.5/250 microtunnels. The dashed white line represents the position where the number of axons is quantified and red boxes are enlargements showing axonal growth in the axon chamber (c). d) Quantification of the number of axons in the axon chambers, showing that there are significantly more axons in the chambers with 3.5 μm high microtunnels than in those with 1 μm high microtunnels for both human and rat neurons. Data are presented as the mean + SD, and ten axon chambers from two independent experiments are analyzed for both cell types. Statistical significance is determined with an independent samples *t*-test; *** $p < 0.001$. The scale bar is 50 μm in all images.

extension and passage of axons, and the number of chambers occupied by axons increased significantly over time for each microtunnel size ($p < 0.001$; Figure S1a, Supporting Information). The axons reached the axon chambers fastest for the tunnels with dimensions of 3.5/100 and 3.5/250, resulting in 100%

occupancy on day 8 (Figure 2b and Figure S1a, Supporting Information). Axon chamber occupancy was significantly lower for devices with 1 μm high tunnels compared with that for devices with 3.5 μm high tunnels when the tunnel length was the same (1/100 versus 3.5/100, $p < 0.001$; 1/250 versus 3.5/250,

$p < 0.001$; 1/500 versus 3.5/500, $p < 0.05$ on days 6 and 8, and 1/250 versus 3.5/250, $p < 0.05$; 1/500 versus 3.5/500, $p < 0.01$ on day 15; Figure 2b). Furthermore, in the chambers with 1 μm high tunnels, occupancy was significantly higher in shorter tunnels (1/100 versus 1/500, $p < 0.01$; 1/250 versus 1/500, $p < 0.05$ on day 6, and 1/100 versus 1/500, $p < 0.01$; 1/250 versus 1/500, $p < 0.01$ on day 8; Figure 2b). The calculation of the total axon counts in the axon chambers with tunnel heights of 1 and 3.5 μm revealed a significantly higher number of axons with the higher tunnels ($p < 0.001$; Figure 2c,d). To verify that the results were independent of the cell line used, human iPSC (hiPSC)-derived neurons (line 10 212.EURCCs) were used in the same experimental setup. The results showed cell migration and good extension of axons from the cell seeding area towards the entry of the microtunnels (Figure S2a, Supporting Information). Similar to the results observed for the hESC-derived neurons, the axon chamber occupancy was dependent on the microtunnel height and length, and significantly higher occupancy was detected with higher tunnels (e.g., on day 6: 1/100 versus 3.5/100 $p < 0.001$; 1/250 versus 3.5/250, $p < 0.001$; 1/500 versus 3.5/500, $p < 0.01$; Figure S2b, Supporting Information) and shorter tunnels (e.g., on day 6: 1/100 versus 1/250, $p < 0.01$; 1/100 versus 1/500, $p < 0.001$; 3.5/100 versus 3.5/500, $p < 0.001$; 3.5/250 versus 3.5/500, $p < 0.05$; Figure S2b, Supporting Information). The axon chamber occupancy also increased significantly over time for each microtunnel size ($p < 0.001$; Figure S2c, Supporting Information). Furthermore, the number of axons in the axon chambers was significantly higher for 3.5 μm high tunnels than for 1 μm tunnels (Figure S2d,e, Supporting Information). Thus, cell behavior within the devices was similar for neurons differentiated from two different hPSC lines.

As microfluidic tunnel devices have been extensively used with primary rodent neurons, we cultured primary rat cortical neurons in the microtunnel testing devices to observe their behavior compared to that of human neurons. Rat neurons did not show remarkable migration out of the cell seeding area, but their processes extended towards the microtunnels, and the entry of the microtunnels of all the devices had a dense neurite network within ≈ 7 days (Figure 2a). Similar to their human counterparts, rat neuronal axons traversed the microtunnels of all six different dimensions, and for each size, the axon chamber occupancy increased significantly over time ($p < 0.001$; Figure S1b, Supporting Information). However, the results for axon chamber occupancy for different tunnel sizes were not as clear as those obtained with human neurons. Regarding the tunnel height, there was a trend toward earlier occupancy for higher microtunnels, but a significant difference was detected only for a tunnel length of 250 μm (1/250 versus 3.5/250, $p < 0.05$ on day 8; Figure 2b). Comparison of the tunnel lengths revealed a significantly higher axon chamber occupancy for 3.5/250 tunnels compared to 3.5/500 tunnels ($p < 0.05$ on days 6 and 8; Figure 2b). Similar to the results observed for human neurons, axon chambers with higher microtunnels had significantly more rat neuronal axons ($p < 0.001$; Figure 2c,d).

Taken together, the results show that axon extension of human PSC-derived and rat primary neurons through the microtunnels was dependent on the cross-sectional area and length of the tunnels. Based on the results, a tunnel height of

3.5 μm , a length of 250 μm , and a width of 10 μm could be recommended for successful axonal growth and isolation.

2.2. A Viable Neuronal Culture is Maintained in a Compartmentalized Microfluidic Device

In addition to allowing the robust extension of axons, the appropriate restriction of neuronal soma migration through microtunnels is needed for precise axonal compartmentalization. Nuclear DAPI staining was performed for human and rat neurons cultured in the microtunnel testing devices to evaluate the number of neuronal somas that migrated through the microtunnels (Figure 3a). Devices with the six different combinations of tunnel dimensions were examined on day 16, and devices with tunnels with dimensions of 3.5/250 were examined also on day 30. For the hPSC-derived neurons (hESC line Regea 08/017), no cell somas were detected in the axon chambers with 1 μm high microtunnels regardless of the tunnel length (Figure 3b). For the 3.5 μm high microtunnels, lengths of 100 and 250 μm permitted the migration of cell somas, but the numbers of migrated somas were remarkably low even after a culture time of 30 days (Figure 3b). Similar findings were observed for neurons derived from hiPSCs (line 10 212.EURCCs), verifying that this phenomenon was not cell line-dependent (Figure S3a,b, Supporting Information). For the rat neurons, no somas were detected in the axon chambers regardless of the tunnel dimensions (representative image of a device with dimensions of 3.5/250 is shown in Figure 3a).

To verify the viability and neuronal phenotype of cells, viability/cytotoxicity assay and immunocytochemical staining were performed. According to calcein-AM staining, both human and rat neurons remained viable for at least 30 days in the neuron compartments and axon chambers, and only a few dead cells (EtHD-1 positive) were observed, which is similar to that observed for the control cultures (Figure 3c and Figure S3c, Supporting Information). Immunostaining confirmed that the neurons maintained their neuronal characteristics (Figure 3d and Figure S3d, Supporting Information). Furthermore, only NF-H (neurofilament heavy)-positive axons were detected in the axon chambers, whereas MAP-2 (microtubule-associated protein 2)-positive dendrites were restricted to the neuronal compartment, as observed on days 16 and 30 (Figure 3d), confirming that only axons were present in the axon chambers.

2.3. Azobenzene-Based Topographical Guidance of the Growth of Neuronal Processes

Topographical features have been shown to enhance the structural organization of hPSC-derived neurons.^[34–37] Hence, we exploited light-induced topographical patterning in an azobenzene-containing material, Disperse Red 1 molecular glass (DR1-glass),^[38] as a novel approach to guide the growth of hPSC-derived neurons. Human PSC-derived neurons (hESC line Regea 08/023) were cultured on flat DR1-glass, which was found to be cytocompatible with these cells and to support similar cell growth and behavior as in control cultures (Figure 4a and Figure S4a, Supporting Information).

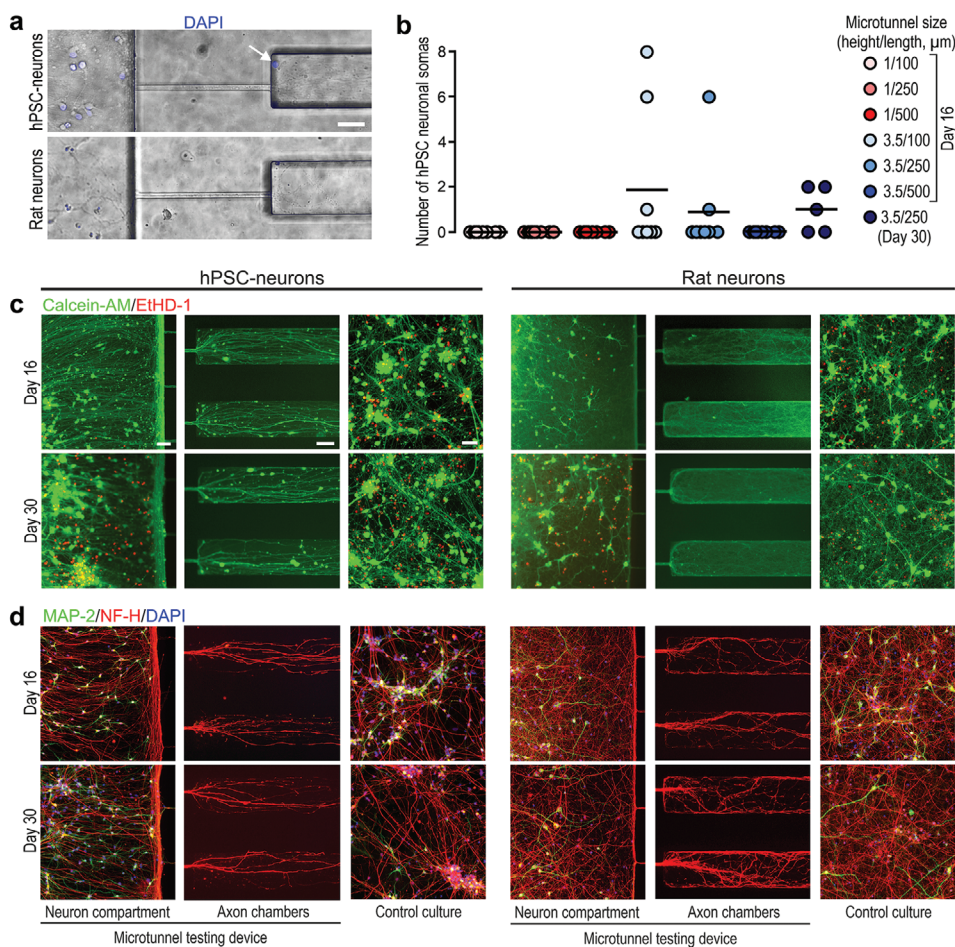


Figure 3. A viable neuronal culture is maintained in the microtunnel testing device. a) Representative images of DAPI staining in the device with 3.5/250 microtunnels on day 16. A migrated hPSC-derived (hESC line Regea 08/017) neuronal soma in the axon chamber is shown with an arrow. Rat neurons did not migrate into axon chambers. b) Number of human neuronal somas in the axon chambers (15 chambers) of one assay unit in the microtunnel testing device with different microtunnel sizes, as calculated using the nuclear stain DAPI. The data are shown as scatter dot plots with a line at the mean, and 5–10 assay units from two independent experiments are analyzed. c,d) Representative images of human and rat neurons cultured in the device with 3.5/250 microtunnels and on the control coverslip, which are analyzed for c) viability/cytotoxicity (calcein AM/EtHD-1) and d) staining of the neuronal markers MAP-2 and NF-H. The scale bar is 50 μm in all images.

Topographical patterns were generated by interference lithography on the DR1-glass films.^[39,40] Briefly, half of a coherent laser beam is reflected by a mirror onto the photosensitive material, interfering with the other half incident directly onto the film surface, creating a pattern of light with periodicity dependent on the angle between the (half)-beams. The azobenzene isomerization in bright regions of the interference pattern activates the migration of the material, leading to a deformation of the surface that replicates the sinusoidal light pattern. Atomic force microscopy (AFM) confirmed very regular sinusoidal grooves with a ≈ 300 nm depth and a 1 μm periodicity (Figure 4b,c). Neurons cultured on the patterned DR1-glass showed normal morphology, and their processes extended in the direction of the patterned nanogrooves (Figure 4d).

Human PSC-derived neurons cultured for seven days on the patterned and flat DR1-glass films and on control coverslips exhibited normal neuronal characteristics, as evaluated by NF-H and MAP-2 stainings (Figure 4e-f and Figure S4b, Supporting Information). According to the quantitative

orientation analysis, both NF-H-positive axons and MAP-2-positive dendrites were evenly distributed in all directions on the flat DR1-glass and control coverslips (Figure 4g). On the patterned DR1-glass, the majority of NF-H-positive axons (66%) and MAP-2-positive dendrites (63%) were aligned within a $\pm 30^\circ$ angle related to the direction of the patterned nanogrooves (Figure 4g). The coherency of the NF-H-positive axons and MAP-2-positive dendrites was significantly higher on the patterned DR1-glass than on the flat DR1-glass and control coverslips ($p < 0.001$; Figure 4h), indicating the robust alignment of neuronal processes on the topographical nanogrooves. There was no significant difference between the coherency of NF-H-positive axons and MAP-2-positive dendrites on the patterned DR1-glass (Figure 4h), suggesting that axons and dendrites respond similarly to these nanotopographies with respect to their alignment. An equivalent experiment with hiPSC-derived neurons (line 10 212.EURCCs) showed similar results (Figure S5, Supporting Information) and further confirmed that the topographical patterning of DR1-glass can guide and

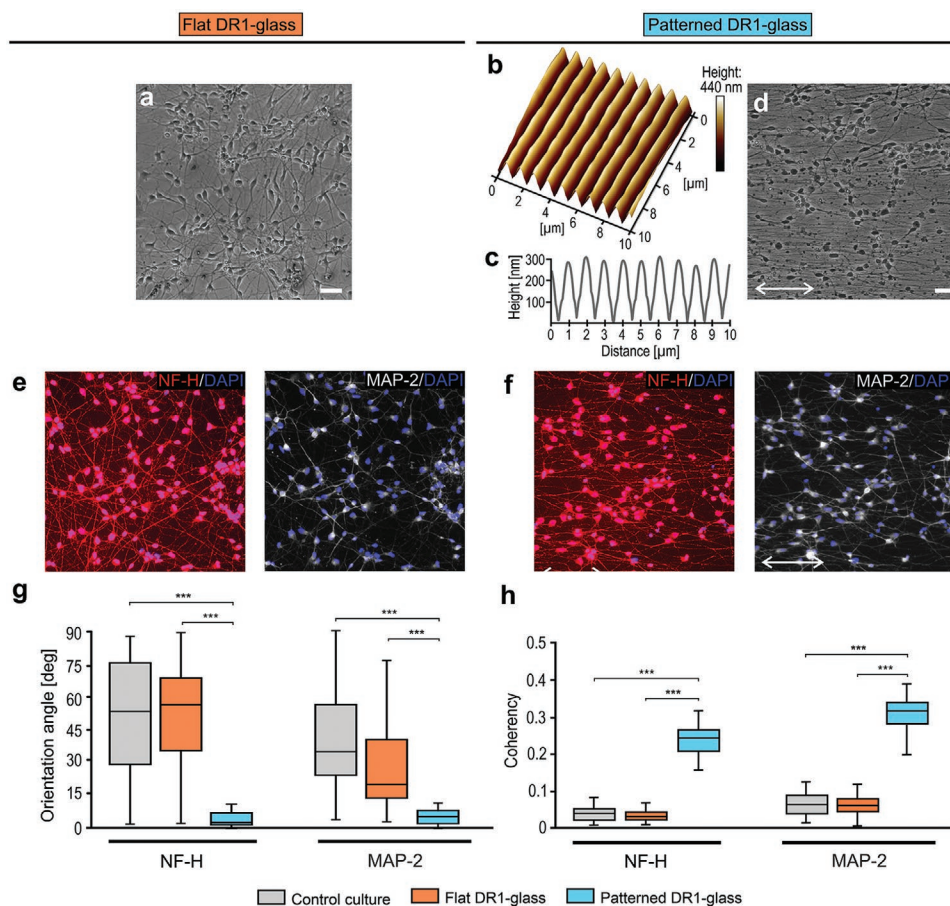


Figure 4. Nanotopography on DR1-glass guides the growth of hPSC-derived neurons (hESC line Regea 08/023). a) A phase-contrast image of neurons cultured on flat DR1-glass for 7 days. b) A 3D projection and c) a central cross-sectional profile of the patterned nanogrooves on the DR1-glass characterized by AFM. d) A phase-contrast image of neurons cultured on patterned DR1-glass for 7 days, showing the tendency of neuronal processes to extend parallel to the direction of the patterned grooves. The two-way arrow indicates the direction of the grooves. e, f) Representative images of NF-H and MAP-2 staining of neurons cultured on the e) flat and f) patterned DR1-glass for 7 days. The two-way arrow indicates the direction of the grooves. g) Box plots with min-max whiskers of the orientation angle distributions for NF-H and MAP-2 on control coverslip, flat and patterned DR1-glass, as determined with OrientationJ Distribution analysis. The horizontal axis of the images in (e, f) is defined as 0°. h) Coherency analysis performed with OrientationJ Measure for neurons cultured on the flat and patterned DR1-glass and on the control coverslip, showing the significantly higher anisotropy of NF-H- and MAP-2-positive processes on the patterned DR1-glass. The data are shown as box plots with min-max whiskers. For (g, h), statistical analysis is performed using the Kruskal–Wallis method and Dunn–Sidak post-hoc test, *** $p < 0.001$. In (g, h), a total of 40 ROIs (40 single images obtained with a 10× objective) from 2 independent experiments are examined. The scale bar is 50 μm in all images.

control the growth of hPSC-derived neurons. Furthermore, viability/cytotoxicity assay was performed for human PSC-derived neurons (hESC line 08/023) cultured on the patterned and flat DR1-glass films and on control coverslips for seven days. The neurons showed similar viability (Calcein-AM positive) and no increased cell death (EtHD-1 positive) was observed on different growth surface verifying the biocompatibility of DR1-glass with human PSC-derived neurons (Figure S6, Supporting Information).

2.4. Integration of Topographical Patterns with Compartmentalized Microfluidic Chip Results in Superior Axonal Alignment

Our recently developed microfluidic device, the 3D3C chip (Figure 5a), enables the robust isolation of rat axons in a specific compartment, as shown previously.^[41] Here, as a result

of the optimization of the microtunnel size, tunnel dimensions of 3.5 μm (height) \times 250 μm (length) \times 10 μm (width) were integrated into the 3D3C chip to achieve both maximal human axon growth and maximal soma restriction. Human neurons (hESC line 08/023) were seeded into the neuron compartments of the chip, and the axons successfully traversed the microtunnels into the middle axon compartment. Although the axons showed robust extension, they tended to turn right while extending and thus did not show direct alignment across the rather sizable compartment (length 3 mm \times width 4 mm) (Figure 5b, b').

To achieve the directional growth of axons across the axon compartment, we integrated the topographical guidance on the DR1-glass into the 3D3C chip. Sinusoidal nanotopographies were generated by mask-aided interference lithography on the DR1-glass within an area matching the size of the axon compartment, and the 3D3C chip was manually bonded to

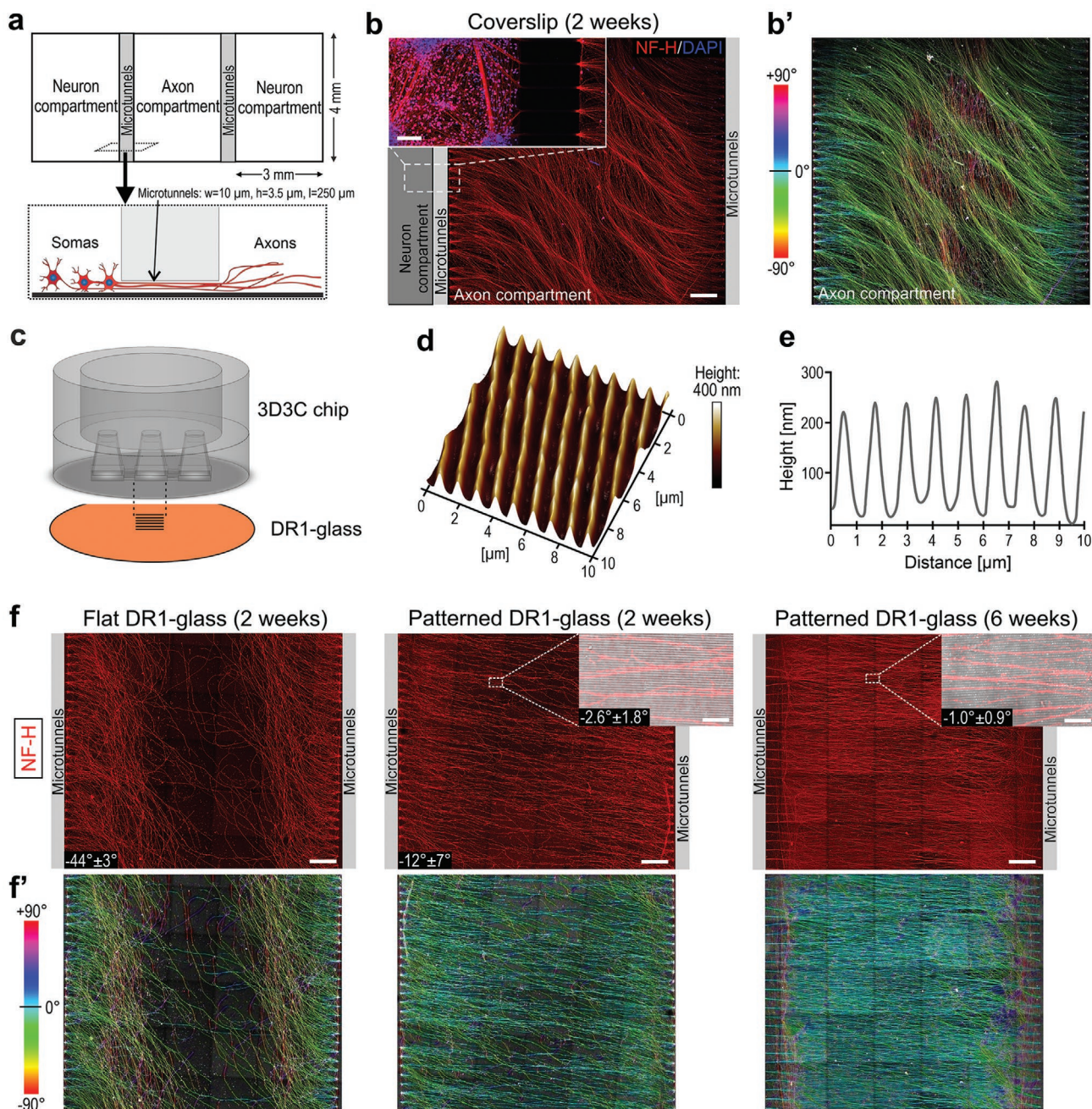


Figure 5. Human PSC-derived neurons (hESC line Regea 08/023) show superior axonal alignment in the compartmentalized microfluidic 3D3C chip with topographical patterns on DR1-glass. a) Schematic illustration of the 3D3C chip used for compartmentalized axonal culture. The chip consists of two neuron compartments and an axon compartment located between the neuron compartments that are interconnected with them by 40 microtunnels. The cross-sectional view of the microtunnel area illustrates the spatial isolation of axons from their somas by microtunnels. w = width, h = height, l = length. b) Staining of NF-H in neurons cultured on the 3D3C chip with a coverslip and b') a color-coded image of the NF-H staining created by OrientationJ showing the non-directed extension of axons in the axon compartment of the 3D3C chip. c) Sinusoidal grooves are generated on the DR1-glass corresponding to the area that matched the axon compartment of the 3D3C chip. The direction of the patterned nanogrooves on the DR1-glass, as characterized by AFM. d) A 3D projection and e) a central cross-sectional profile of the patterned nanogrooves on the DR1-glass, as characterized by AFM. f) Representative images of NF-H staining in the axon compartment of the 3D3C chip on flat and patterned DR1-glass and f') color-coded images of the orientation characterization, as analyzed with OrientationJ. The average orientation angle of axons in the axon compartment on the flat DR1-glass is $-44^\circ \pm 3^\circ$ and on the patterned DR1-glass $-12^\circ \pm 7^\circ$ at the 2-week time point. Three entire axon compartments of individual chips from both groups are analyzed with OrientationJ Measure, and the length of the axon compartment and the direction of the grooves are defined to be at a 0° orientation. Scaled-up images in (f) show the NF-H-stained axons and bright-field image of the patterned grooves underneath. The average deviation angle between the axons and patterns is $-2.6^\circ \pm 1.8^\circ$ at the two-week time point and $-1.0^\circ \pm 0.9^\circ$ at the six-week time point. To determine this, 14–20 ROIs (images obtained with a 60 \times objective) from three to four independent chips are analyzed with OrientationJ Measure. In (b) and (f), the colors represent the orientation angles in the range between -90° and $+90^\circ$, where 0° is the horizontal axis in the image. Scale bars: 500 μm in the axon compartment images in both (b) and (f); 200 μm and 10 μm in the scaled-up images in (b) and (f), respectively.

the patterned DR1-glass (Figure 5c). AFM characterization confirmed the intended topographical features of the patterns (≈ 300 nm deep grooves with a period of $1 \mu\text{m}$) (Figure 5d,e). Human neurons were cultured in the 3D3C chips. In the axon compartment with flat DR1-glass (Figure 5f, f'), axons showed similar nondirected extension and a wide range of orientation angles, as observed on the glass coverslip (Figure 5a, a'), whereas, on the patterned DR1-glass, the axons obviously extended in an aligned orientation (Figure 5f, f'). According to the analysis performed at the two-week time-point, the average orientation angle of axons in the axon compartment with flat DR1-glass was $-44^\circ \pm 3^\circ$, and that in the axon compartment with patterned DR1-glass was significantly smaller ($-12^\circ \pm 7^\circ$; $p = 0.002$). As the length of the axis of the axon compartment and the direction of the patterns in the analysis were defined to be at 0° orientation, this result clearly indicates the improvement of axonal alignment by the photoinscribed nanotopography (Figure 5f, 5f'). Comparison of the main orientation angles between the NF-H-positive axons and the patterns underneath revealed that the axons grown on the patterned DR1-glass had a remarkable preference for the direction of the nanotopography, as the average deviation angle was only $2.6^\circ \pm 1.8^\circ$ at the two-week time point (Figure 5f). Axons maintained their aligned orientation parallel to the underlying topography for up to six weeks, and the average deviation angle was as small as $1.0^\circ \pm 0.9^\circ$ (Figure 5f, 5f'). The results indicate that topographical patterning on azobenzene-containing material can be integrated into the microfluidic chip to provide the robustly directed and efficiently aligned axon extension of hPSC-derived neurons in long-term cultures for several weeks.

2.5. OGD Induces Axonal Damage for the Aligned Axons

We used the developed 3D3C chip model integrated with the patterned DR1-glass to model axonal damage that is known to occur in ischemic stroke. The OGD-reperfusion treatment, a well-known inducer for neuronal damage, was performed after neurons were cultured on the chips for two weeks (Figure 6a). β -tubulin staining in the axon compartment of the 3D3C chip showed the aligned orientation of the axons and that the OGD treatment disrupted the integration of microtubules in the axons indicated by the dotted staining pattern and more disintegrated axons compared to non-treated cells (Figure 6b). Quantification of the microtubular disintegration by calculating an axonal degeneration index in β -tubulin-stained axons in the whole axonal compartment revealed that the OGD-treated axons were damaged significantly when compared to the non-treated axons ($p < 0.05$, Figure 6c).

The results indicate that the OGD induces axonal damage for hPSC-derived neurons that have aligned axonal orientation in the isolated axonal microenvironment in the microfluidic chip. Thus, modeling and analyzing axonal damage is feasible in the developed chip and the aligned axonal network enables facilitated analysis of, for example, axonal outgrowth, de- and regeneration and axonal trafficking compared to models with random axonal orientation.

3. Discussion

Axonal dysfunction and degeneration are common pathological features of many CNS diseases and traumas.^[1,2] To model

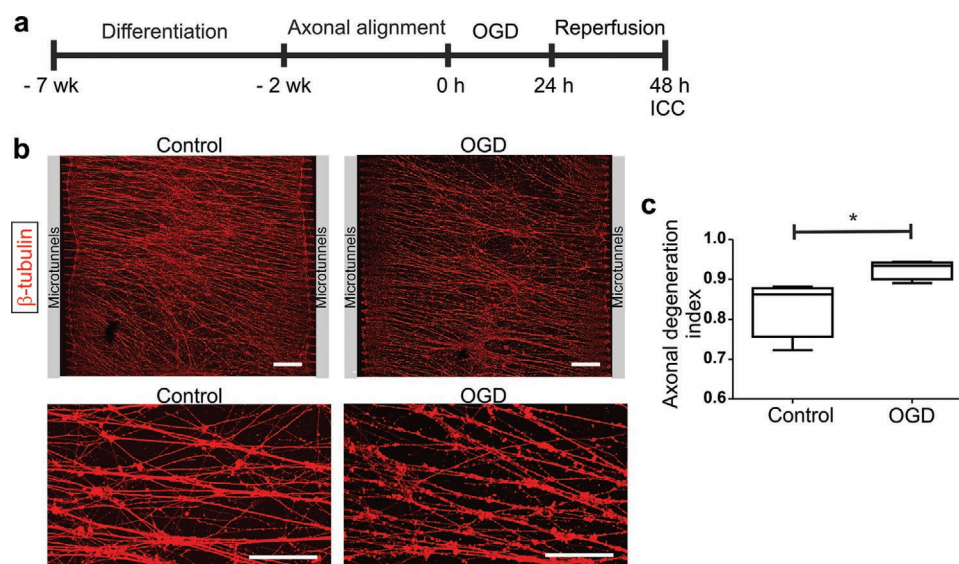


Figure 6. OGD induces axonal damage of human PSC-derived neurons (hESC line Regea 08/023) cultured in the 3D3C chip integrated onto patterned DR1-glass. a) Timeline for the cell culture and OGD and reperfusion (R) treatment. Human PSCs are first differentiated to neurons for five weeks, thereafter neurons are cultured on 3D3C chip for two weeks prior to OGD treatment to form aligned axonal network in the axon compartment. Thereafter, OGD/R is performed for cells to induce axonal damage. b) Representative images of β -tubulin staining of OGD/R-treated cells and respective control in the axon compartments of the 3D3C chip at 2-week timepoint. Scaled-up images of β -tubulin staining showed dotted staining pattern and fragmented axons in OGD/R-treated neurons indicating axonal damage. c) Quantification of microtubular disintegration by calculating axonal degeneration index from β -tubulin stained images in (b) showed higher axonal disintegration in OGD-treated group when compared to control group. The data are shown as box plots with min-max whiskers. Statistical analysis is performed using the Mann Whitney U test, $*p < 0.05$. Four chips per group are analyzed from one independent experiment. Scale bars: $500 \mu\text{m}$ in the axon compartment images and $50 \mu\text{m}$ in the scaled-up images.

disease processes in vitro, axon-targeted research is remarkably facilitated by the ability to achieve directional axonal growth in an isolated microenvironment which demands different technological solutions.^[10–12] Therefore, in this study, we investigated the requirements for achieving robust directional axonal growth with separation from neuronal somas in a microfluidic PDMS-based compartmentalized device. Furthermore, we studied the applicability of the light-induced topographical patterning of an azobenzene-containing material, DR1-glass, for directed axonal guidance. We created a multicompartment microfluidic chip integrated with compartment-specific photo-inscribed nanotopography and verified the functionality of the chip with hPSC-derived neurons, which showed the robust alignment of axonal orientation in an isolated microenvironment during extended long-term culture for six weeks. Furthermore, we showed that induction of axonal damage, modeling, for example, ischemic stroke, is feasible in the designed device.

The advantages of microfluidic multicompartment devices rely on microtunnels and their dimensions of which control axon extension and soma migration to allow the separation of axons and somas within their dedicated compartments with distinct microenvironments. Previous studies of microtunnel devices have predominantly used rodent neurons, whereas only a handful of studies have utilized human neurons. Overall, previous studies have lacked systematic comparisons of different microtunnel dimensions for the optimization of axonal growth and isolation to prevent interference from somas.^[10,17,22–31] Here, we performed an extensive screening and quantitative analysis of two different microtunnel heights (1 and 3.5 μm) and three lengths (100, 250, and 500 μm) in six different combinations by using human PSC-derived and rat primary cortical neurons. Our results demonstrated that the somas of rat neurons were unable to penetrate through microtunnels of any dimensions, which apparently was a reflection of minimal cell migration within the devices. Human PSC-derived neurons, which in general have higher migration capacity, were able to migrate through the 3.5 μm high tunnels yet to a very minor extent, whereas 1 μm high tunnels completely prevented soma migration. Further analysis revealed that the 3.5 μm high tunnels allowed robust axonal extension, whereas the number of extended axons was remarkably low for the 1 μm high tunnels for both human and rat neurons. Our previous study using rat dorsal root ganglion (DRG) neurons showed limited axonal extension in tunnels with smaller cross-sectional area,^[41] and a correlation between decreased tunnel width and a reduced axon number has been reported for mouse cortical^[27] and rat hippocampal neurons.^[42] Thus, the cross-sectional area of microtunnels plays an important role in achieving robust axon outgrowth for neurons with different origins, and here, we were able to define a height of 3.5 μm with a cross-sectional area of 35 μm^2 as optimal for both human and rat cortical neurons.

Successful axon compartmentalization in a microfluidic device is determined by the absence of not only somas but also of other neuronal processes, dendrites. As dendrites are shorter than axons, the length of the microtunnels allows the isolation of axons from dendrites. A previous study showed that the dendrites of rodent cortical and hippocampal neurons could traverse 150 μm long tunnels (height = 3 μm ,

width = 10 μm), whereas with a 450 μm tunnel length, axonal isolation from dendrites was achieved in two weeks of culture.^[20] Another study using rat cortical neurons reported that a 200 μm long tunnel (height = 2.5 μm , width = 15 μm) was sufficient for axon-dendrite separation in two weeks of culture.^[21] In this study, we did not detect the passage of MAP-2-positive dendrites of rat or human neurons through 250 μm long tunnels (height = 3.5 μm , width = 10 μm) even at the 30-day follow-up time point, thus indicating successful axonal isolation. Importantly, our results showed that axons tended to occupy axon chambers with shorter tunnels faster than those with longer tunnels. Consistent with our data, axonal isolation for rat cortical neurons has been achieved more quickly with shorter tunnels.^[21] Even though axons can grow long distances, and 750–900 μm long tunnels have been used for axonal isolation,^[20–23,42–44] the use of shorter tunnels has the benefit of promoting the formation of an axonal microenvironment as early as possible. Thus, our defined microtunnel dimensions, 3.5 μm (height) \times 250 μm (length) \times 10 μm (width), maximize the experimental time window, which is critical when utilizing hPSC-derived neurons that have a slower functional maturation process than rodent cells^[45] as well as when utilizing primary cells that have a restricted culture time. As an added bonus, a longer experimental time enables the study of slowly progressive CNS diseases in vitro.

For detailed and precise axonal studies, it is preferable that isolated axons would grow in aligned, unidirectional manner, which is not achieved at least for human hPSC neurons without additional surface modifications. Surface topography has a potent influence on neuronal orientation, and obtaining directional axonal growth in vitro is of great importance when studying axon-specific phenomena.^[33–36,46,47] Despite the growing interest and need for utilizing hPSC-derived neurons for in vitro disease modeling,^[6] only a handful of studies have reported the responses of hPSC-derived neurons to topographical surface features.^[34–37] In the present study, we took advantage of light-induced nanotopography on an azobenzene-containing material, DR1-glass, and showed, to the best of our knowledge, for the first time, that DR1-glass is cytocompatible with the culture of hPSC-derived neurons as it has been shown with other cells such as Epithelial Madin–Darby canine kidney type II (MDCK II) cells.^[40] Importantly, the formed nanotopography in DR1-glass guides neuronal processes into an aligned morphology. We used sinusoidal gratings with a 1 μm period and a \approx 300 nm depth. In earlier reports, similar \approx 1 μm periodic gratings with various depths in azobenzene-containing materials have provided effective guidance for the alignment and migration of rat neuron-like PC12 cells and human primary astrocytes.^[48–50] Previous studies of hPSC-derived neurons have reported neuronal alignment along topographical gratings on PDMS and Nafion substrates fabricated by soft lithography.^[34–37] These techniques provide rectangular groove/ridge gratings that have different geometry compared to the sinusoidal-shaped nanogratings we produced on DR1-glass. On a PDMS substrate, a 2 μm groove/ridge width with a 2 μm depth^[35,36] and a 1 μm groove/ridge width with a 560 nm depth have promoted the axonal alignment of human neurons;^[34] a Nafion substrate with an 800 nm groove/ridge width produced similar results.^[37] Altogether, these

results suggest that different grating geometries and dimensions produced with different fabrication techniques and variable materials can be utilized to achieve axonal alignment of hPSC-derived neurons.

In addition to aligned axonal growth, the isolated axon microenvironment further facilitates targeted axonal biology studies, as shown with rat CNS neurons.^[33] In the present study, we utilized our previously developed compartmentalized PDMS device, the 3D3C chip, in which isolated and aligned axonal growth of rat DRG neurons has been achieved.^[41] As hPSC-derived neurons failed to extend their axons directly into the axon compartment of the chip, we integrated light-induced topographical nanogratings that were fabricated on DR1-glass into the chip. This is a novel approach for combining sinusoidal topographical gratings and microfluidic axon compartmentalization. No previous studies have shown the coupling of axonal isolation and the formation of an aligned axonal network of hPSC-derived neurons. In the system, we demonstrated directional axonal growth that was separated from somas and dendrites for hPSC-derived neurons. Importantly, we performed an extended, long-term follow-up experiment that verified the maintenance of the created aligned axonal microenvironment for at least six weeks, enabling researchers to tackle research questions that require long-term culture. Compartmentalization of rat neuronal axons and their simultaneous directed growth was achieved earlier in a PDMS device utilizing partially sealed patterned PDMS microgrooves.^[33] Our approach is different and combines two distinct techniques, topographical guidance on DR1-glass and microfluidic compartmentalization in a PDMS device, which display several advantages. Topographical patterns on DR1-glass are created by single-step light irradiation, which is an easy and quick fabrication method that results in highly reproducible pattern features.^[38,51] These topographies can be erased and manipulated after fabrication by additional light irradiation,^[52,53] which can be performed also in the presence of living cells.^[54,55] This peculiar characteristic of light-responsive azobenzene-based materials allows the spatiotemporal manipulation of surface topography, providing opportunities to study, for example, human neuronal differentiation and axonal biology in health and disease in an unprecedented way. Altogether, our results demonstrated the formation of an extensive and robust aligned axonal network in a combined system comprising a compartmentalized microfluidic chip with topographical gratings on DR1-glass. Furthermore and importantly, we showed that the induction and quantitative analysis of axonal damage are feasible in the developed system. The OGD-induced axonal damage, most widely used model for ischemic stroke, was successfully analyzed from the aligned axons in the axonal compartment. Previous reports describing axonal damage in chip models have mainly focused on analyzing single or few axons in small microtunnels^[31] or in non-aligned axonal compartments.^[56] Here, the analysis of axons in axonal compartment in their aligned orientation, compared to random orientation, enables facilitated analysis of, for example, axonal outgrowth, de- and regeneration and axonal trafficking and thus, the developed system widens and eases ways to perform detailed analysis related to axonal biology.

4. Conclusion

In this study, we showed that successful isolation of axons from somas and dendrites combined with the robust axonal outgrowth of hPSC-derived and rat primary cortical neurons in a compartmentalized microfluidic PDMS device is greatly influenced by the cross-sectional area and the length of the separating microtunnels. Furthermore, we created an hPSC-derived neuron-based axonal model consisting of a compartmentalized PDMS microtunnel chip integrated with photoinscribed nanotopography on light-responsive, azobenzene-based molecular glass. Thanks to the combination of microtunnels and surface topography, robust directional axonal growth in an isolated microenvironment and OGD-induced axonal damage was demonstrated in the model. This novel in vitro model enables enhanced axon-targeted research with the possibility of controlling surface topography during experiments in real-time. These advances may lead to the enhanced discovery of disease-specific mechanisms targeting axons and thus contribute to the development of novel treatments for CNS diseases associated with axonal dysfunction and degeneration.

5. Experimental Section

Design and Fabrication of Microfluidic Devices: To find the optimal microtunnel dimensions for the isolation of axons from their somas, a microfluidic device called a microtunnel testing device containing two identical assay units was designed (Figure 1a). One assay unit consisted of a neuron compartment connected to 15 axon chambers by microtunnels with six different sizes (Figure 1b,c), which were tested for their effects on axonal isolation. The neuron compartment (width = 3 mm, length = 3.1–3.5 mm) included a cell seeding area (\varnothing 3 mm) created by a punching tool. The axon chambers (width = 100 μ m, length = 1 mm, height = 100 μ m) enabled the observation of axonal extension and the migration of neuronal somas through the microtunnels. The axon chambers were further connected to a compartment with a similar inlet as the punched cell seeding area in the neuron compartment to ensure the complete diffusion of staining reagents throughout the axon chamber during the analyses. The devices were fabricated from PDMS (10:1 mass ratio with the curing agent SYLGARD 184, Dow Corning, Midland, MI) by replica molding using an SU-8 mold.^[16] During the mold fabrication, standard multilayer SU-8 photolithography^[17] was used with SU-8 5 photoresist (micro resist technology GmbH, Berlin, Germany) to produce 1 and 3.5 μ m high microtunnels, and SU-8 3050 (micro resist technology GmbH) was used for 100 μ m high features. The devices were separated from the 3 mm high replica using a \varnothing 15 mm punching tool.

For the establishment of isolated and aligned axonal cultures, a previously described PDMS microfluidic device was used.^[41] This microfluidic device, called the 3D3C chip (Figure 5a), consists of two neuron compartments (length = 3 mm, width = 4 mm), which were interconnected by 40 microtunnels (length = 250 μ m, width = 10 μ m, height = 3.5 μ m) to an axon compartment in the middle (length = 3 mm, width = 4 mm). The 3D3C chips were produced from PDMS (SYLGARD 184) using a combination of SU-8 photolithography and 3D printing for mold fabrication as previously reported^[41] with few modifications. Here, to increase the surface quality of the 3D-printed parts of the mold and to reduce fabrication costs, the parts were fabricated from epoxy resin (Black V4, Formlabs) with stereolithography (SLA) instead of using stainless steel with selective laser melting. The 3D parts were printed with a Form 2 SLA printer (Formlabs, Somerville, MA). After printing, the parts were sonicated (Wash, Formlabs) in isopropanol for 20 min and cured twice in a UV oven (Cure, Formlabs) for 20 min at 60 °C; they were cured once before removal of the supports and once after removal.

Table 1. Details of experiments.

	Microtunnel dimension testing	Patterning experiment without device	Isolated axonal culture	Control culture
Device	Microtunnel testing device (Figure 1a–c)	–	3D3C chip (Figure 5a)	–
Coverslip size [Ø]	15 mm	15 mm	24 mm	13 mm
Coverslip type	Plain coverslip	DR1-glass film	Plain coverslip DR1-glass film	Plain coverslip
hPSC-neurons Cell seeding amount	20 000 (in cell seeding area)	13 500 (as a 60 µL droplet)	60 000 (in neuron compartments)	50 000
Rat neurons Cell seeding amount	7 000–20 000 (in cell seeding area)	–	–	50 000

The 3D parts were attached to the SU-8 mold using a glue gel (Loctite Super Glue Power Easy Gel, Henkel, Dusseldorf, Germany).

Preparation and Characterization of Disperse Red 1 Molecular Glass Films: Glass coverslips (Ø15 mm and Ø24 mm) were washed twice in acetone in an ultrasonication bath for 10 min and then dried under a fume hood before the spin coating process. The azobenzene-containing material used, Disperse Red 1 molecular glass (DR1-glass; Solaris Chem. Inc., Quebec, Canada), was dissolved in chloroform (5% w/v). The solution was spun over the coverslips by using a Laurell spin coater (Laurell Technologies Corp., North Wales, PA) at 1500 rpm for 30 s. Samples were patterned with the interference lithography technique in Lloyd's mirror configuration. An optically pumped semiconductor laser with a continuous wave output of 488 nm with a 2 W maximum output power (Genesis CX 488-2000, Coherent Inc., Santa Clara, CA) was used with a Lloyd's mirror configuration with circular polarization to project an interference pattern of light on the DR1-glass films, thus inducing the formation of surface relief gratings using an intensity of 300 mW cm⁻². The pattern period Λ of 1 µm was given by Equation (1):

$$\Lambda = \frac{\lambda}{2 \sin \vartheta} \quad (1)$$

where λ is the laser wavelength and ϑ (set to 14°) is the angle between the incident beam and the mirror. For the inscription of localized patterns that were to be integrated with the 3D3C microfluidic chip, a photomask was prepared by gluing a black adhesive film with a central opening (3 mm × 2.5 mm) on a clean glass slide. The DR1-glass film was covered with the photomask and fixed to one of the mirror's edges.

A Dimension 3100 AFM (Veeco Instruments Inc., Plainview, NY) was used to characterize the patterned DR1-glass films. A silicon tip (PPP-NCH, PointProbe Plus Non-Contact/Tapping Mode-High Resonance Frequency, NanoWorld AG, Neuchâtel, Switzerland) with a spring constant of 42 N m⁻¹ and a nominal resonance frequency of 330 kHz was used in tapping mode in air at room temperature (RT).

Preparation of Microfluidic Devices and Disperse Red 1 Molecular Glass Films for Cell Culture: The sizes and types of glass coverslips used in the cell culture experiments were shown in Table 1. Plain coverslips were sterilized with 70% EtOH, and the coverslips with DR1-glass films were sterilized with UV light for 30 min before use. For hPSC-derived neurons, the coverslips used for the microtunnel testing devices, 3D3C chips, and control cultures were coated with poly-L-ornithine (PO; ≈12 µg cm⁻²; Sigma-Aldrich, St. Louis, MO) by spreading PO over the whole coverslip. For the patterning experiments that did not involve the device, coating was performed with a 60 µL droplet of 65 µg mL⁻¹ PO. For primary rat cortical neurons, the whole coverslip surface was coated with poly-D-lysine (PDL; ≈5 µg cm⁻²; Sigma-Aldrich). Both substrates were diluted in boric acid buffer, and coating was performed for 1.5 h at +37 °C. Thereafter, the uncoated substrates were washed with sterile H₂O, and the coverslips were allowed to air dry.

The microtunnel testing devices were treated with oxygen plasma in a Pico plasma system (4 min at 50 W; Diener electronic GmbH + Co. KG, Ebhausen, Germany) for sterilization and to make them hydrophilic, which would facilitate the inflow of laminin and cell culture medium into the microscale features. The 3D3C chips were polyvinylpyrrolidone (PVP)-coated and thus permanently hydrophilic.^[41,57] The sterilization of the PVP-coated chips was performed by immersing the chips in 70% ethanol and air-drying them thereafter. The microtunnel testing devices

and the 3D3C chips were reversibly bonded to the PO- and/or PDL-coated coverslips. In the case of the patterned DR1-glass films, the 3D3C chips were manually aligned under a microscope to match the axon compartment on the patterned area. For hPSC-derived neurons, the microtunnel testing devices and the 3D3C chips were filled with mouse laminin (mLN, 20 µg mL⁻¹; Sigma-Aldrich) or human recombinant laminin-521 (LN521, 30 µg mL⁻¹; BioLamina, Sundbyberg, Sweden). The microtunnel testing devices used for primary rat cortical neurons were filled with culture medium immediately after bonding. For the control culture of hPSC-derived neurons, ≈1.5 µg cm⁻² of mLN or ≈2 µg cm⁻² of LN521 was used to coat the whole PO-coated coverslip surface. For the patterning experiments without the 3D3C chip, a 60 µL droplet of 15 µg mL⁻¹ LN521 was used. Laminin coating was carried out overnight at +4 °C, and the devices were housed in 24-well or 6-well plates.

hPSCs and Differentiation of Neurons: The hESC lines Regea 08/017 and 08/023^[58] and hiPSC line 10 212.EURCCs^[59] were used for neuronal differentiation. The lines were derived at the Faculty of Medicine and Health Technology, Tampere University, Finland. The approval from the Finnish Medicines Agency to conduct research with human embryos (Dnro 1426/32/300/05) and supportive statement from the regional ethics committee of Pirkanmaa Hospital District for the derivation, culture, and differentiation of hESCs (R05116) and hiPSCs (R08070) were obtained prior to the research. The hESC and hiPSC lines were expanded in feeder-free culture on LN521 in E8 medium (Thermo Fisher Scientific, Waltham, MA) as previously described.^[60] The pluripotency of the lines was confirmed regularly, and all cultures maintained normal karyotypes and were free of mycoplasma.

Neuronal differentiation was performed according to a method reported earlier.^[45] Briefly, at day 32, the cells were plated for experiments as described in Table 1 in neural maturation medium consisting of a 1:1 mixture of D-MEM/F12 (with GlutaMAX) and Neurobasal medium, 0.5% N2, 1% B27 with retinoic acid, 0.5 mM GlutaMAX, 0.5% NEEA, 50 µM 2-mercaptoethanol (all from Thermo Fisher Scientific), 2.5 µg mL⁻¹ insulin (Sigma), 20 ng mL⁻¹ brain-derived neurotrophic factor (BDNF, R&D Systems), 10 ng mL⁻¹ glial-derived neurotrophic factor (GDNF, R&D Systems), 500 µM dibutyryl-cyclic AMP (db-cAMP, Sigma-Aldrich), 200 µM ascorbic acid (AA, Sigma-Aldrich) and 0.1% penicillin/streptomycin (Thermo Fisher Scientific). ROCK inhibitor (10 µM; Sigma-Aldrich) was included in the medium used for cell passaging but omitted thereafter, and the medium was changed every two to three days. During neural induction, the coating substrate was Matrigel (Corning Inc., Corning, NY) or sequential coating with PO (100 µg mL⁻¹) and LN521 (15 µg mL⁻¹). After induction, sequential coating with PO (100 µg mL⁻¹) and LN521 (15 µg mL⁻¹) or mLN (15 µg mL⁻¹) were used.

Primary Rat Cortical Culture: Cortical tissue was extracted from Wistar rat embryos at embryonic day E17-E18, and the primary cortical cells were prepared as previously described.^[61] All experimental protocols were approved by the local ethic committee (County Administrative Board of Southern Finland, ESAVI/10300/04.10.07/2016) to conduct the described procedures. All experiments were performed according to institutional guidelines and regulations (University of Helsinki internal license number: KEK17-016). The culture medium consisted of Neurobasal medium, 2% B27 with retinoic acid, 2 mM GlutaMAX, and 1% penicillin/streptomycin (all from Thermo Fisher Scientific). Cells were plated for the experiments as described in Table 1 and cultured with media changes every two to three days.

Analysis of Axon Extension: A phase-contrast microscope (Nikon Eclipse TE2000-S, Nikon Corp., Tokyo, Japan) was used to follow the growth of axons in the microtunnel testing devices. To study axon extension through microtunnels of different sizes, the number of axon chambers containing axons was counted every 1–4 days until all 15 axon chambers in one assay unit contained axons or 14 days (rat neurons) or 16 days (human neurons) had elapsed. To determine the number of axons entering axon chambers, individual axons were counted manually based on the phase contrast images at a distance of 300 μm from the microtunnels (the dashed lines in Figure 2c and Figure S2d, Supporting Information).

Nuclear Staining of Living Cells: The number of neuronal somas migrating through microtunnels into the axon chambers of the microtunnel testing devices was determined based on nuclear staining of living cells using 4',6-diamidino-2 phenylindole (DAPI). Cells cultured in the devices for 15 days were incubated in culture medium containing DAPI (1 $\mu\text{g mL}^{-1}$; Sigma-Aldrich) at +37 $^{\circ}\text{C}$ for 24 h. After washing once with PBS, the cells were immediately examined with an Olympus IX51 fluorescence microscope equipped with a DP30BW camera (Olympus Corp., Tokyo, Japan), and the number of DAPI-positive somas in the axon chambers was calculated.

Cell Viability Assay: To determine the viability of neurons, a LIVE/DEAD Viability/Cytotoxicity Kit for mammalian cells (Thermo Fisher Scientific) was used for microtunnel testing devices and their control cultures on coverslips. Cells cultured in the microtunnel testing devices and control cultures grown on coverslips for 16 and 30 days were incubated in culture medium containing 0.1 μM calcein AM (detection of live cells, emission \approx 515 nm) and 0.5 μM ethidium homodimer-1 (EtHD-1, detection of dead cells, emission \approx 617 nm) at +37 $^{\circ}\text{C}$ for 1 h. After replacing the medium with PBS, the cells were examined with an Olympus IX51 fluorescence microscope. Cells cultured on the DRI-glass films and coverslips for seven days were incubated in culture medium containing 0.5 μM CellTrace Calcein Red-Orange, AM (emission \approx 590 nm, Thermo Fisher Scientific) or 0.5 μM EtHD-1 (emission \approx 590 nm, Thermo Fisher Scientific) at +37 $^{\circ}\text{C}$ for 30 min. EtHD-1-stained cells were imaged immediately after incubation, while CellTrace Calcein Red-Orange-stained cells were imaged after washing the cells twice with fresh media. Death cells were quantified as the ratio of the number of EtHD-1 positive cells to the total number of cells in the same region. The number of EtHD-1 positive cells was counted automatically by using ImageJ watershed function after median filtering and binarization. The total number of cells was estimated from phase-contrast microscopy images captured during viability assay. Estimation was done semi-automatically by using ImageJ particle analyzer after initial background correction, image binarization, and subsequent median filtering.

Immunocytochemistry: Immunocytochemical staining was performed for cells cultured in the microtunnel testing devices by first removing the PDMS from the coverslips. The cells on these coverslips, the cells cultured on the DRI glass films, and the control cultures were fixed with 4% PFA for 15 min, and staining was performed as previously described.^[62] For the 3D3C chips, staining was performed without removing the PDMS from the coverslips, and the cells were fixed by replacing half of the medium in the neuron and axon compartments with 4% PFA (\approx 15 μl) and incubating for 45 min at RT. The staining procedure for the 3D3C chips was performed according to a published protocol^[62] with increased times for washing steps (30 min instead of 5 min) and secondary antibody incubation (1.5 h instead of 1 h). In addition, the final wash with PB was replaced by a wash with PBS. All the samples were mounted with ProLong Gold Antifade Mountant (Thermo Fisher Scientific) that included DAPI and imaged using an Olympus IX51 fluorescence microscope or an LSM780 laser scanning confocal microscope equipped with a Quasar spectral GaAsP detector (Carl Zeiss, Oberkochen, Germany). The primary antibodies used were mouse anti-neurofilament heavy (NF-H, 1:500; Sigma-Aldrich), chicken anti-NF-H (1:250; GenScript, Piscataway, NJ), rabbit anti-microtubule-associated protein 2 (MAP-2, 1:200; Sigma-Aldrich), and rabbit anti-beta-III tubulin (1:500; GenScript), and the secondary antibodies were Alexa Fluor 488 anti-rabbit, Alexa Fluor 568 anti-mouse, Alexa Fluor 568 anti-chicken and Alexa Fluor 647 anti-rabbit (1:400) (all from Thermo Fisher Scientific).

Orientation Analysis: Fluorescence images immunostained with NF-H and MAP-2 were analyzed using plugins in ImageJ software (version 1.52e) to determine the orientation of the neuronal processes on the patterned and flat DRI-glass films and on the control coverslips. For the quantitative analysis of the distribution of orientation, the plugin OrientationJ Distribution was used.^[63] The analysis was automatized using a custom macro script. Processes aligned parallel to the horizontal axis of the image (direction of the patterned grooves) were defined to be at a 0 $^{\circ}$ orientation, and the other directions obtained angles in the range between -90° and $+90^{\circ}$. The results were shown within the range from 0 $^{\circ}$ to 90 $^{\circ}$, as the absolute values of the orientation angles were considered. Weighted histograms showing the distribution of orientations of the NF-H-positive axons and MAP-2-positive dendrites were built based on the normalized frequencies of the pixel orientations at 15 $^{\circ}$ intervals. The anisotropy of the NF-H- and MAP-2-stained processes was quantified by evaluating the coherency using the OrientationJ Measure plugin.^[63–65] This parameter measures the morphological anisotropy of the image features in a defined region of interest; coherency = 0 indicates an isotropic image, whereas coherency >0 (maximum value = 1) indicates the presence of a dominant direction. Once again, the analysis was automatized using a custom macro script. The plugin OrientationJ Analysis^[66] was used for the qualitative visual analysis of the directionality of the NF-H-positive axons in the axon compartment of the 3D3C chip. OrientationJ Measure was used to calculate the main orientation angle of axons in the axon compartment of the 3D3C chip on the flat and patterned DRI-glass and to determine the deviation angle of NF-H-positive axons compared to the patterns underneath.

OGD and Reperfusion: To induce axonal damage in vitro, cells were cultured in the 3D3C chips integrated onto patterned DRI-glass and during the first two weeks, aligned axonal network in the axonal compartment was let to form. Thereafter, cells were treated with optimized OGD treatment as recently reported.^[67] First, neurons were washed with glucose-free DMEM (Thermo Fisher Scientific) and thereafter incubated in glucose-free DMEM in a humidified oxygen control CO₂ incubator (HeraCell, Thermo Fisher Scientific) with 1% O₂, 5% CO₂, and 94% N₂ for 24 h at 37 $^{\circ}\text{C}$. After 24 h, cells were reperused by removing the medium and replacing it with neural maturation medium containing glucose and the cells were further incubated for 24 h in 95% air/5% CO₂ (Figure 6a). Control chips were washed and incubated in the neural maturation medium containing glucose, respectively, under normoxic conditions for 24 h in 95% air/5% CO₂ (HeraCell).

Integration of microtubules in axons was quantified by using a previously described method.^[56] According to the method, an axonal degeneration index was calculated from the confocal images of β -tubulin-stained axons in the entire axon compartment of the 3D3C chip. The images were binarized and fragmented by using ImageJ watershed function. The fragmented axons were calculated using ImageJ particle analyzer plugin with the following parameters: size (pixels)—0–15000 and circularity—0.30–1.00. The axonal degeneration index was then calculated as the ratio of fragmented axon area over the total axon area.

Statistical Analysis: Analysis of the axon extension for the different microtunnel sizes and the axonal degeneration index were performed using the Mann-Whitney U-test, analysis of axon extension over time for each microtunnel size with the Friedman test, and analysis of the number of axons entering axon chambers with the independent samples *t*-test using SPSS Statistics (v.25; IBM Corp., Armonk, NY). The Kruskal–Wallis method and Dunn–Sidak post-hoc test were used for the analysis of coherency data for the NF-H- and MAP-2-stained processes using MATLAB software. The number of samples used for each analysis was presented in the corresponding figure legend. A *p*-value less than 0.05 was considered statistically significant.

Supporting Information

Supporting Information is available from the Wiley Online Library or from the author.

Acknowledgements

The authors thank Arla Tanner and Anniina Brofeldt for assistance in the microtunnel dimension testing experiments, Marlitt Viehrig for assistance in the manufacturing of the microfluidic devices and Hanna Mäkelä and Eija Hannuksela for technical assistance with cell maintenance. Prof. Eero Castrén and the Neuronal Cell Culture Unit at the University of Helsinki are acknowledged for providing the primary rat cortical culture. The work was supported by the Imaging Facility and iPS Cells Facility (Faculty of Medicine and Health Technology, Tampere University). The authors also thank Biocenter Finland for the support of Imaging and iPS cells facilities. This work was supported by the Academy of Finland (grants 296415, MR; 312414, SN; 312411, PK; 332693, FEK; and 330707, SH), Business Finland (Human Spare Parts project, SN and PK), the Finnish Cultural Foundation (CF, SH). AP and CF also gratefully acknowledge Emil Aaltonen Foundation for financial support. F.E.K. also acknowledges Orion Research Foundation for financial support, S.H. for The Päivikki and Sakari Sohlberg Foundation, and R.M. for Orion foundation and Instrumentarium Science Foundation.

Conflict of Interest

The authors declare no conflict of interest.

Data Availability Statement

Original data can be shared after reasonable inquiry from the authors.

Keywords

azobenzene, human pluripotent stem cells, light-responsive materials, microfluidics, surface relief gratings, topographic guidance

Received: January 15, 2021

Revised: March 12, 2021

Published online:

- [1] N. Egawa, J. Lok, K. Washida, K. Arai, *Transl. Stroke Res.* **2017**, *8*, 14.
- [2] N. Salvadores, M. Sanhueza, P. Manque, F. A. Court, *Front. Neurosci.* **2017**, *11*, 451.
- [3] J. Sandoe, K. Eggan, *Nat. Neurosci.* **2013**, *16*, 780.
- [4] Y. Avior, I. Sagi, N. Benvenisty, *Nat. Rev. Mol. Cell Biol.* **2016**, *17*, 170.
- [5] J. Mertens, M. C. Marchetto, C. Bardy, F. H. Gage, *Nat. Rev. Neurosci.* **2016**, *17*, 424.
- [6] A. Farkhondeh, R. Li, K. Gorshkov, K. G. Chen, M. Might, S. Rodems, D. C. Lo, W. Zheng, *Drug Discovery Today* **2019**, *24*, 992.
- [7] C. Czaniecki, T. Ryan, M. G. Stykel, J. Drolet, J. Heide, R. Hallam, S. Wood, C. Coackley, K. Sherriff, C. D. C. Bailey, S. D. Ryan, *Proc. Natl. Acad. Sci. U. S. A.* **2019**, *116*, 14280.
- [8] K. R. Denton, C. Xu, X. Li, *Methods Mol. Biol.* **2016**, *1353*, 309.
- [9] J. N. Sleigh, A. M. Rossor, A. D. Fellows, A. P. Tosolini, G. Schiavo, *Nat. Rev. Neurol.* **2019**, *15*, 691.
- [10] E. Neto, L. Leitão, D. M. Sousa, C. J. Alves, I. S. Alencastre, P. Aguiar, M. Lamghari, *J. Neurosci.* **2016**, *36*, 11573.
- [11] S. Halldorsson, E. Lucumi, R. Gómez-Sjöberg, R. M. T. Fleming, *Biosens. Bioelectron.* **2015**, *63*, 218.
- [12] R. Siddique, N. Thakor, *J. R. Soc., Interface* **2014**, *11*, 20130676.
- [13] R. B. Campenot, *Proc. Natl. Acad. Sci. U. S. A.* **1977**, *74*, 4516.
- [14] B. Campenot, K. Lund, D. L. Senger, *J. Cell Biol.* **1996**, *135*, 701.
- [15] B. L. MacInnis, R. B. Campenot, *Science* **2002**, *295*, 1536.
- [16] D. C. Duffy, J. C. McDonald, O. J. Schueller, G. M. Whitesides, *Anal. Chem.* **1998**, *70*, 4974.
- [17] A. M. Taylor, S. W. Rhee, C. H. Tu, D. H. Cribbs, C. W. Cotman, N. L. Jeon, *Langmuir* **2003**, *19*, 1551.
- [18] J. W. Park, B. Vahidi, A. M. Taylor, S. W. Rhee, N. L. Jeon, *Nat. Protoc.* **2006**, *1*, 2128.
- [19] A. Pelkonen, R. Mzezewa, L. Sukki, T. Rynnänen, J. Kreutzer, T. Hyvärinen, A. Vinogradov, L. Aarnos, J. Leikkala, P. Kallio, S. Narkilahti, *Biosens. Bioelectron.* **2020**, *168*, 112553.
- [20] A. M. Taylor, M. Blurton-Jones, S. W. Rhee, D. H. Cribbs, C. W. Cotman, N. L. Jeon, *Nat. Methods* **2005**, *2*, 599.
- [21] J. Park, H. Koito, J. Li, A. Han, *Biomed. Microdevices* **2009**, *11*, 1145.
- [22] A. M. Taylor, D. C. Dieterich, H. T. Ito, S. A. Kim, E. M. Schuman, *Neuron* **2010**, *66*, 57.
- [23] X. Lu, J. S. Kim-Han, K. L. O'Malley, S. E. Sakiyama-Elbert, *J. Neurosci. Methods* **2012**, *209*, 35.
- [24] R. Cartoni, G. Pekkurnaz, C. Wang, T. L. Schwarz, Z. He, *PLoS One* **2017**, *12*, e0184672.
- [25] R. Habibey, A. Golabchi, S. Latifi, F. Difato, A. Blau, *Lab Chip* **2015**, *15*, 4578.
- [26] A. Lesniak, D. Kilinc, A. Blasiak, G. Galea, J. C. Simpson, G. U. Lee, *Small* **2019**, *15*, 1803758.
- [27] J. Peyrin, B. Deleglise, L. Saias, M. Vignes, P. Gougis, S. Magnifico, S. Betuing, M. Pietri, J. Caboche, P. Vanhoutte, J. Viovy, B. Brugg, *Lab Chip* **2011**, *11*, 3663.
- [28] N. Lee, J. W. Park, H. J. Kim, J. H. Yeon, J. Kwon, J. J. Ko, S. Oh, H. S. Kim, A. Kim, B. S. Han, S. C. Lee, N. L. Jeon, J. Song, *Mol. Cells* **2014**, *37*, 497.
- [29] R. L. Bigler, J. W. Kamande, R. Dumitru, M. Niedringhaus, A. M. Taylor, *Sci. Rep.* **2017**, *7*, 611.
- [30] J. W. Kamande, T. Nagendran, J. Harris, A. M. Taylor, *Front. Bioeng. Biotechnol.* **2019**, *7*, 84.
- [31] T. Hyvärinen, S. Hagman, M. Ristola, L. Sukki, K. Veijula, J. Kreutzer, P. Kallio, S. Narkilahti, *Sci. Rep.* **2019**, *9*, 16944.
- [32] M. Toivanen, A. Pelkonen, M. Mäkinen, L. Ylä-Outinen, L. Sukki, P. Kallio, M. Ristola, S. Narkilahti, *Front. Neurosci.* **2017**, *11*, 606.
- [33] J. Park, S. Kim, S. I. Park, Y. Choe, J. Li, A. Han, *J. Neurosci. Methods* **2014**, *227*, 166.
- [34] L. Song, K. Wang, Y. Li, Y. Yang, *Colloids Surf., B* **2016**, *148*, 49.
- [35] K. K. B. Tan, W. W. M. Lim, C. Chai, M. Kukumberg, K. L. Lim, E. L. K. Goh, E. K. F. Yim, *Sci. Rep.* **2018**, *8*, 9567.
- [36] L. Y. Chan, W. R. Birch, E. K. F. Yim, A. B. H. Choo, *Biomaterials* **2013**, *34*, 382.
- [37] A. Smith, E. Choi, K. Gray, J. Macadangdang, E. Ahn, E. Clark, P. Tyler, M. Laflamme, L. Tung, J. Wu, C. Murry, D. Kim, **2018**.
- [38] R. Kirby, R. G. Sabat, J.-M. Nunzi, O. Lebel, *J. Mater. Chem. C* **2014**, *2*, 841.
- [39] P. Rochon, E. Batalla, A. Natansohn, *Appl. Phys. Lett.* **1995**, *66*, 136.
- [40] C. Fedele, E. Mäntylä, B. Belardi, T. Hamkins-Indik, S. Cavalli, P. A. Netti, D. A. Fletcher, S. Nymark, A. Priimagi, T. O. Ihalainen, *Sci. Rep.* **2020**, *10*, 15329.
- [41] M. Ristola, L. Sukki, M. M. Azevedo, A. I. Seixas, J. B. Relvas, S. Narkilahti, P. Kallio, *J. Micromech. Microeng.* **2019**, *29*, 065009.
- [42] U. Narula, A. Ruiz, M. McQuaide, T. B. DeMarse, B. C. Wheeler, G. J. Brewer, *PLoS One* **2017**, *12*, e0176868.
- [43] B. J. Dworak, B. C. Wheeler, *Lab Chip* **2009**, *9*, 404.
- [44] H. Wu, G. Cheng, Y. Wong, C. Lin, W. Fang, W. Chow, Y. Chang, *Lab Chip* **2010**, *10*, 647.
- [45] T. Hyvärinen, A. Hysalo, F. E. Kapucu, L. Aarnos, A. Vinogradov, S. J. Eglén, L. Ylä-Outinen, S. Narkilahti, *Sci. Rep.* **2019**, *9*, 17125.
- [46] M. J. Aebersold, H. Dermutz, C. Forró, S. Weydert, G. Thompson-Steckel, J. Vörös, L. Demkó, *Trends Anal. Chem.* **1982**, *78*, 60.
- [47] C. Simitzi, A. Ranella, E. Stratakis, *Acta Biomater.* **2017**, *51*, 21.

- [48] H. Baac, J. Lee, J. Seo, T. H. Park, H. Chung, S. Lee, S. J. Kim, *Mater. Sci. Eng., C* **2004**, *24*, 209.
- [49] R. Barillé, R. Janik, S. Kucharski, J. Eyer, F. Letournel, *Colloids Surf., B* **2011**, *88*, 63.
- [50] R. Barillé, P. Codron, G. Mabileau, F. Manero, R. Mallet, S. Zielinska, E. Ortyl, J. Eyer, F. Letournel, *Open Biomed. Eng. J.* **2018**, *12*, 92.
- [51] O. R. Bennani, T. A. Al-Hujran, J. Nunzi, R. G. Sabat, O. Lebel, *New J. Chem.* **2015**, *39*, 9162.
- [52] X. L. Jiang, L. Li, J. Kumar, D. Y. Kim, S. K. Tripathy, *Appl. Phys. Lett.* **1998**, *72*, 2502.
- [53] J. Vapaavuori, R. H. A. Ras, M. Kaivola, C. G. Bazuin, A. Priimagi, *J. Mater. Chem. C* **2015**, *3*, 11011.
- [54] V. Y. Chang, C. Fedele, A. Priimagi, A. Shishido, C. J. Barrett, *Adv. Opt. Mater.* **2019**, *7*, 1900091.
- [55] C. Rianna, L. Rossano, R. H. Kollarigowda, F. Formiggini, S. Cavalli, M. Ventre, P. A. Netti, *Adv. Funct. Mater.* **2016**, *26*, 7572.
- [56] V. Sundaramoorthy, D. Green, K. Locke, C. M. O'Brien, M. Dearnley, J. Bingham, *PLoS Pathog.* **2020**, *16*, e1008343.
- [57] S. Hemmilä, J. V. Cauich-Rodríguez, J. Kreuzer, P. Kallio, *Appl. Surf. Sci.* **2012**, *258*, 9864.
- [58] H. Skottman, *In Vitro Cell. Dev. Biol.: Anim.* **2010**, *46*, 206.
- [59] M. Kiamehr, A. Klettner, E. Richert, A. Koskela, A. Koistinen, H. Skottman, K. Kaarniranta, K. Aalto-Setälä, K. Juuti-Uusitalo, *Int. J. Mol. Sci.* **2019**, *20*, 3773.
- [60] H. Hongisto, T. Ilmarinen, M. Vattulainen, A. Mikhailova, H. Skottman, *Stem Cell Res. Ther.* **2017**, *8*, 291.
- [61] M. Sahu, O. Nikkilä, S. Lâgas, S. Kolehmainen, E. Castrén, *Neuronal Signaling* **2019**, *3*, NS20180207.
- [62] R. S. Lappalainen, M. Salomäki, L. Ylä-Outinen, T. J. Heikkilä, J. A. K. Hyttinen, H. Pihlajamäki, R. Suuronen, H. Skottman, S. Narkilahti, *Regener. Med.* **2010**, *5*, 749.
- [63] R. Rezakhaniha, A. Agianniotis, J. T. C. Schrauwen, A. Griffa, D. Sage, C. V. C. Bouten, van de Vosse, F. N. , M. Unser, N. Stergiopoulos, *Biomech. Model. Mechanobiol* **2012**, *11*, 461.
- [64] E. Fonck, G. G. Feigl, J. Fasel, D. Sage, M. Unser, D. A. Rüfenacht, N. Stergiopoulos, *Stroke* **2009**, *40*, 2552.
- [65] T. D. Clemons, M. Bradshaw, P. Toshniwal, N. Chaudhari, A. W. Stevenson, J. Lynch, M. Fear, F. M. Wood, K. S. Iyer, *RSC Adv.* **2018**, *8*, 9661.
- [66] Z. Püspöki, M. Storath, D. Sage, M. Unser, *Adv Anat Embryol Cell Biol* **2016**, *219*, 69.
- [67] M. Juntunen, S. Hagman, A. Moisan, S. Narkilahti, S. Miettinen, *Stem Cells Int.* **2020**, *2020*, 8841026.